Glassy orientational dynamics of rodlike molecules near the isotropic-nematic transition

Biman Jana, Dwaipayan Chakrabarti, and Biman Bagchi*
Solid State and Structural Chemistry Unit, Indian Institute of Science, Bangalore 560012, India
(Received 31 August 2006; revised manuscript received 19 February 2007; published 25 July 2007)

We investigate the single-particle orientational dynamics of rodlike molecules across the isotropic-nematic transition in computer simulations of a family of model systems of thermotropic liquid crystals. Several remarkable features of glassy dynamics are on display including nonexponential relaxation, dynamical heterogeneity, and non-Arrhenius temperature dependence of the orientational relaxation time. In order to obtain a *quantitative* measure of glassy dynamics in line with the established methods in supercooled liquids, we construct a relaxation time versus scaled inverse temperature plot and demonstrate that one can indeed define a "fragility index" for thermotropic liquid crystals that depends on density and aspect ratio. The values of the fragility parameter are surprisingly in the range observed for glass-forming liquids. A plausible correlation between the energy landscape features and the observed fragility is discussed.

DOI: 10.1103/PhysRevE.76.011712 PACS number(s): 61.30.−v, 61.20.Lc, 64.70.Pf

I. INTRODUCTION

Thermotropic liquid crystals exhibit exotic phase behavior upon temperature variation. In the isotropic phase, liquid does not have any long-range translational or orientational order. The nematic phase is rich with a long-ranged orientational order but lacks translational order. The isotropic-nematic (I-N) phase transition, which is believed to be weakly first order in nature with certain characteristics of the continuous transition, has been a subject of immense attention in condensed matter physics and material sciences [1,2]. In contrast, the dynamics of thermotropic liquid crystals has been much less studied, the focus being mostly on the long-time behavior of orientational relaxation near the I-N transition [1]. A series of optical Kerr effect (OKE) measurements have, however, recently studied collective orientational relaxation in the isotropic phase near the I-N transition over a wide range of time scales [3]. The dynamics have been found to be surprisingly rich, the most intriguing feature being the power-law decay of the OKE signal at short-to-intermediate times [3]. The relaxation scenario appears to be strikingly similar to that of supercooled molecular liquids [4], even though the latter do not undergo any thermodynamic phase transition. Although analogous dynamics has been investigated in subsequent studies [5,6], a quantitative estimation of the glassy dynamics of rodlike molecules near the I-N transition still eludes us.

The prime objective of this paper is to provide a quantitative measure of the glassy dynamics near the I-N transition. To this end, we have undertaken molecular dynamics simulations of a family of model systems consisting of rodlike molecules across the I-N transition in search of glassy behavior. Given the involvement of the phase transition to an orientationally ordered mesophase upon lowering the temperature, we choose to probe the single-particle orientational dynamics. We have defined a "fragility index" and explored plausible correlation of the features of the underlying energy landscape with the observed fragility in analogy with supercooled liquids.

*bbagchi@sscu.iisc.ernet.in

II. MODEL AND DETAILS OF THE SIMULATION

The systems we have studied consist of ellipsoids of revolution. The Gay-Berne (GB) pair potential [7], which is well established to serve as a model potential for systems of thermotropic liquid crystals, has been employed. The GB pair potential, which uses a single-site representation for each ellipsoid of revolution, is an elegant generalization of the extensively used isotropic Lennard-Jones potential to incorporate anisotropy in both the attractive and the repulsive parts of the interaction [7,8]. Indeed, the repulsive part of the GB potential produces ellipsoidal shape. In the GB pair potential, ith ellipsoid of revolution is represented by the position $\mathbf{r}_i$ of its center of mass and a unit vector $\mathbf{e}_i$ along the long axis of the ellipsoid. The interaction potential between two ellipsoids of revolution i and j is given by

$$U_{ij}^{GB}(\mathbf{r}_{ij},\mathbf{e}_i,\mathbf{e}_j) = 4\epsilon(\hat{\mathbf{r}}_{ij},\mathbf{e}_i,\mathbf{e}_j)(\rho_{ij}^{-12} - \rho_{ij}^{-6}), \tag{1}$$

where

$$\rho_{ij} = \frac{r_{ij} - \sigma(\hat{\mathbf{r}}_{ij},\mathbf{e}_i,\mathbf{e}_j) + \sigma_{ss}}{\sigma_{ss}}. \tag{2}$$

Here σ_{ss} defines the thickness or, equivalently, the separation between the two ellipsoids of revolution in a side-by-side configuration, r_{ij} is the distance between the centers of mass of the ellipsoids of revolution i and j, and $\hat{\mathbf{r}}_{ij}=\mathbf{r}_{ij}/r_{ij}$ is a unit vector along the intermolecular separation vector $\mathbf{r}_{ij}$. The molecular shape parameter σ and the energy parameter ϵ both depend on the unit vectors $\mathbf{e}_i$ and $\mathbf{e}_j$ as well as on $\hat{\mathbf{r}}_{ij}$ as given by the following set of equations:

$$\sigma(\hat{\mathbf{r}}_{ij},\mathbf{e}_i,\mathbf{e}_j) = \sigma_0\left[1 - \frac{\chi}{2}\left\{\frac{(\mathbf{e}_i\cdot\hat{\mathbf{r}}_{ij} + \mathbf{e}_j\cdot\hat{\mathbf{r}}_{ij})^2}{1+\chi(\mathbf{e}_i\cdot\mathbf{e}_j)} + \frac{(\mathbf{e}_i\cdot\hat{\mathbf{r}}_{ij} - \mathbf{e}_j\cdot\hat{\mathbf{r}}_{ij})^2}{1-\chi(\mathbf{e}_i\cdot\mathbf{e}_j)}\right\}\right]^{-1/2}, \tag{3}$$

with $\chi=(\kappa^2-1)/(\kappa^2+1)$ and

$$\epsilon(\hat{\mathbf{r}}_{ij},\mathbf{e}_i,\mathbf{e}_j) = \epsilon_0[\epsilon_1(\mathbf{e}_i,\mathbf{e}_j)]^{\nu}[\epsilon_2(\hat{\mathbf{r}}_{ij},\mathbf{e}_i,\mathbf{e}_j)]^{\mu}, \tag{4}$$

where the exponents μ and ν are adjustable parameter and

$$\epsilon_1(\mathbf{e}_i,\mathbf{e}_j) = [1-\chi^2(\mathbf{e}_i\cdot\mathbf{e}_j)^2]^{-1/2} \tag{5}$$

and

$$\epsilon_2(\hat{\mathbf{r}}_{ij},\mathbf{e}_i,\mathbf{e}_j) = 1-\frac{\chi'}{2}\left[\frac{(\mathbf{e}_i\cdot\hat{\mathbf{r}}_{ij}+\mathbf{e}_j\cdot\hat{\mathbf{r}}_{ij})^2}{1+\chi'(\mathbf{e}_i\cdot\mathbf{e}_j)}+\frac{(\mathbf{e}_i\cdot\hat{\mathbf{r}}_{ij}-\mathbf{e}_j\cdot\hat{\mathbf{r}}_{ij})^2}{1-\chi'(\mathbf{e}_i\cdot\mathbf{e}_j)}\right], \tag{6}$$

with $\chi'=(\kappa'^{1/\mu}-1)/(\kappa'^{1/\mu}+1)$. Here $\kappa=\sigma_{ee}/\sigma_{ss}$ is the aspect ratio of the ellipsoid of revolution, with σ_{ee} denoting the separation between two ellipsoids of revolution in a end-to-end configuration, and $\sigma_{ss}=\sigma_0$ and $\kappa'=\epsilon_{ss}/\epsilon_{ee}$, where ϵ_{ss} is the depth of the minimum of the potential for a pair of ellipsoids of revolution aligned in a side-by-side configuration and ϵ_{ee} is the corresponding depth for the end-to-end alignment. Here ϵ_0 is the depth of the minimum of the pair potential between two ellipsoids of revolution aligned in cross configuration. The GB pair potential defines a family of models, each member of which is characterized by the values chosen for the set of four parameters κ, κ', μ, and ν, and is represented by GB(κ,κ',μ,ν) [8]. Three systems—namely, GB(3, 5, 2, 1), GB(3.4, 5, 2, 1), and GB(3.8, 5, 2, 1)—which differ in the aspect ratio, have been investigated. Molecular dynamics simulations have been performed with each of these systems, consisting of 500 ellipsoids of revolution, in a cubic box with periodic boundary conditions. Each of these systems has been studied along three isochors (ρ=0.31, 0.32, and 0.33 for κ=3.0; ρ=0.25, 0.26, and 0.27 for κ=3.4; ρ=0.215, 0.225, and 0.235 for κ=3.8) at several temperatures, starting from the high-temperature isotropic phase down to the nematic phase across the I-N phase boundary. All quantities are given in reduced units defined in terms of the Gay-Berne potential parameters ϵ_0 and σ_0: length in units of σ_0, temperature in units of $\frac{\epsilon_0}{k_B}$ and time in units of $\left(\frac{\sigma_0^2 m}{\epsilon_0}\right)^{1/2}$, m being the mass of the ellipsoids of revolution. The mass as well as the moment of inertia of each of the ellipsoids of revolution has been set equal to unity. The intermolecular potential is truncated at a distance r_{cut} and shifted such that $U(r_{ij}=r_{cut})=0$, r_{ij} being the separation between two ellipsoids of revolution i and j. The equations of motion have been integrated using the velocity-verlet algorithm with integration time step dt=0.0015 [9]. Equilibration has been done by periodic rescaling of linear and angular velocities of particles. This has been done for a time period of t_q, following which the system has been allowed to propagate with a constant energy for a time period of t_e in order to ensure equilibration upon observation of no drift of temperature, pressure, and potential energy. The data collection has been executed in a microcanonical ensemble. At each state point, local potential energy minimization has been executed by the conjugate gradient technique for a subset of 200 statistically independent configurations. The landscape analysis has been done with a system size of 256 ellipsoids of revolution, which is large enough for having no qualitative change in the results due to the system size [10]. Minimization has been performed with three position coordinates and two Euler angles for each particle, the third Euler angle being redundant for ellipsoids of revolution.

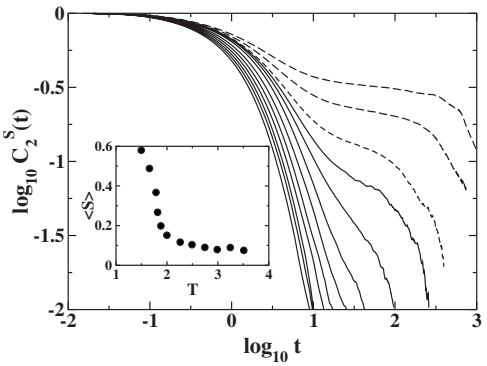

FIG. 1. Time evolution of the single-particle second-rank orientational time correlation function $C_2^s(t)$ in a log-log plot for the system with aspect ratio κ=3. The time dependence is shown at several temperatures (T=3.5, 3.25, 3.0, 2.75, 2.5, 2.25, 2.0, 1.88, 1.82, 1.78, 1.65, and 1.5) across the isotropic-nematic transition along the isochor at density ρ=0.33. The solid lines denote the curves for the high-temperature isotropic phase and the dashed lines for the low-temperature nematic phase. The inset shows the average orientational order parameter $\langle S\rangle$ as a function of temperature.

III. RESULTS AND DISCUSSION

The single-particle second-rank orientational time correlation function (OTCF) $C_2^s(t)$ is defined by

$$C_2^s(t) = \frac{\langle\sum_i P_2(\hat{\mathbf{e}}_i(t)\cdot\hat{\mathbf{e}}_i(0))\rangle}{\langle\sum_i P_2(\hat{\mathbf{e}}_i(0)\cdot\hat{\mathbf{e}}_i(0))\rangle}, \tag{7}$$

where P_2 is the second-rank Legendre polynomial, $\hat{\mathbf{e}}_i$ is the unit vector along the long axis of ith ellipsoid of revolution, and the angular brackets stand for ensemble averaging.

Figure 1 shows the time evolution of the single-particle second rank OTCF for one of the three systems considered here as the temperature is lowered along an isochor from the high-temperature isotropic phase down to the nematic phase across the I-N phase boundary. In the inset, the average orientational order parameter $\langle S\rangle$ is shown as a function of temperature along the isochor [11]. The variation of $\langle S\rangle$ with temperature serves to locate the I-N phase boundary. In the present study, the I-N transition temperature $T_{I\text{-}N}$ is taken as the temperature at which $\langle S\rangle$ of the system is 0.35. For each aspect ratio, three isochors at different densities have been considered. The qualitative behavior has been found to be the same for all the three systems along all the isochors studied (data not shown). The emergence of the power-law decay in the isotropic phase near the I-N transition is evident in all the cases as a universal characteristic of I-N transition [12]. As the I-N phase boundary is crossed upon cooling, the advent of two power-law decay regimes separated by an intervening plateau at short-to-intermediate times imparts a steplike feature to the temporal behavior of the second rank OTCF. Such a feature bears remarkable similarity to what is observed for supercooled liquids as the glass transition is approached from the above [13,14]. While for the supercooled liquid the emergence of the steplike feature in the OTCF is well under-

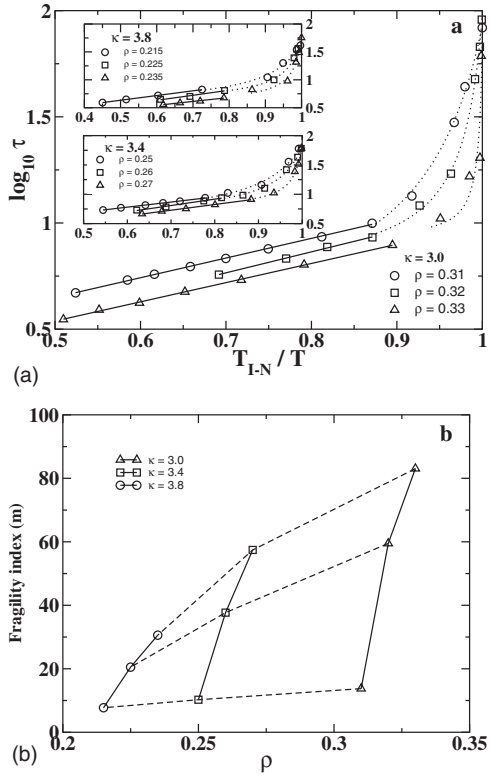

FIG. 2. (a) The orientational correlation time τ in the logarithmic scale as function of the inverse of the scaled temperature, the scaling being done by the isotropic to nematic transition temperature $T_{I\text{-}N}$. For the insets, the horizontal and vertical axis labels read same as that of the main frame and are thus omitted for clarity. Along each isochor, the solid line is the Arrhenius fit to the subset of the high-temperature data and the dotted line corresponds to the fit to the data near the isotropic-nematic phase boundary with the VFT form. (b) The fragility index m shown as a function of density for different aspect ratios. The dashed lines are guide to the eye to illustrate the fact that the dependence of the fragility index on the density is becoming stronger as the aspect ratio becomes smaller.

stood as a consequence of β relaxation, the origin of such a feature observed for liquid crystal defied a reliable explanation.

We estimate the orientational correlation time τ as the time taken for $C_2^s(t)$ to decay by 90%—i.e., $C_2^s(t=\tau)=0.1$. Figure 2(a) shows τ in the logarithmic scale as a function of the inverse temperature along the three isochors for each of the three systems considered. We have scaled the temperature by $T_{I\text{-}N}$ in the spirit of Angell's plot, which displays the shear viscosity (or the structural relaxation time, the inverse diffusivity, etc.) of glass-forming liquids as a function of the inverse of the scaled temperature, the scaling being done in the latter case by the glass transition temperature T_g [15,16]. For all three systems, two distinct features are common: (i) in the isotropic phase far away from the I-N transition, the orientational correlation time τ exhibits the Arrhenius temperature dependence—i.e., $\tau(T)=\tau_0 \exp[E/(k_B T)]$, where the activation energy E and the prefactor τ_0 are both independent of temperature; (ii) in the isotropic phase near the I-N transition, the temperature dependence of τ shows a marked deviation from the Arrhenius behavior and can be well described by the Vogel-Fulcher-Tammann (VFT) equation $\tau(T)=\tau_0 \exp[B/(T-T_{VFT})]$, where τ_0, B, and T_{VFT} are constants, independent of temperature. Again these features bear remarkable similarity with those observed for fragile glass-forming liquid. A non-Arrhenius temperature behavior is taken to be the signature of fragile liquids. For fragile liquids, the temperature dependence of the shear viscosity follows the Arrhenius behavior far above T_g and can be fitted to the VFT functional form in the deeply supercooled regime near T_g [15,16].

The striking resemblance in the dynamical behavior described above between the isotropic phase of thermotropic liquid crystals near the I-N transition and supercooled liquids near the glass transition has prompted us to attempt a quantitative measure of glassy behavior near the I-N transition. For supercooled liquids, one quantifies the dynamics by a parameter called the fragility index which measures the rapidity at which the liquid's properties (such as viscosity) change as the glassy state is approached. In the same spirit [17] that offers a quantitative estimation of the fragile behavior of supercooled liquids, we here define the fragility index m of a thermotropic liquid crystalline system as

$$m = \left. \frac{d \log_{10}(T)}{d(T_{I-N}/T)} \right|_{T=T_{I-N}}. \tag{8}$$

It is clear from the above equation that if $\tau(T)$ follows an Arrhenius temperature dependence, m will be constant throughout the whole temperature range. Figure 2(b) shows the density dependence of the fragility index for the three systems with different aspect ratios. For a given aspect ratio, the fragility index increases with increasing density, the numerical values of the fragility index m being comparable to those of supercooled liquids. For the range of aspect ratios studied here, the dependence of the fragility index on the density is becoming stronger as the aspect ratio becomes smaller.

Another hallmark of fragile glass-forming liquids is spatially heterogeneous dynamics [18] reflected in non-Gaussian dynamical behavior [19]. It is intuitive that the growth of the pseudonematic domains, characterized by local nematic order, in the isotropic phase near the I-N transition would result in heterogeneous dynamics in liquid crystals. We have, therefore, monitored the time evolution of the rotational non-Gaussian parameter (NGP) [20], $\alpha_2^R(t)$, which in the present case is defined as

$$\alpha_2^R(t) = \frac{\langle \Delta \boldsymbol{\phi}^4(t) \rangle}{2\langle \Delta \boldsymbol{\phi}^2(t) \rangle^2} - 1, \tag{9}$$

where

$$\langle \Delta \boldsymbol{\phi}^{2n}(t) \rangle = \frac{1}{N} \sum_{i=1}^{N} \langle |\boldsymbol{\phi}_i(t) - \boldsymbol{\phi}_i(0)|^{2n} \rangle. \tag{10}$$

Here $\boldsymbol{\phi}_i$ is the rotation vector analogous to the position vector $\mathbf{r}_i$ appears in the case of translational NGP of ith ellipsoid of revolution, the change of which is defined by $\Delta \boldsymbol{\phi}_i(t)$

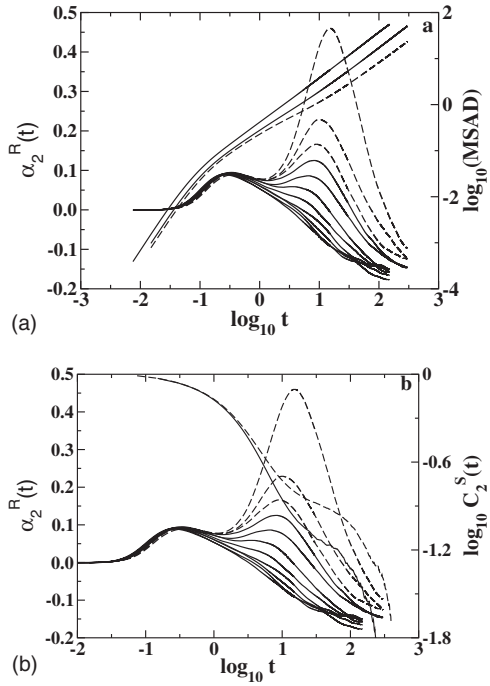

FIG. 3. Time evolution of the rotational non-Gaussian parameter $\alpha_2^R(t)$ in a semilogarithmic plot for the system with aspect ratio $\kappa=3$. The time dependence is shown at several temperatures ($T=3.5$, 3.25, 3.0, 2.75, 2.5, 2.25, 2.0, 1.88, 1.82, 1.78, and 1.5) across the isotropic-nematic (I-N) transition along an isochor at density $\rho=0.33$. (a) On a different scale along the vertical axis (appearing on the right), the time evolution of the mean-square angular deviation $\langle \Delta \boldsymbol{\phi}^2(t) \rangle$ is shown in a log-log plot for three temperatures: the highest temperature studied in the isotropic phase ($T=1.5$) and the other two temperatures ($T=3.0$ and 2.75) that are closest to the I-N transition on either side along with the time evolution of $\alpha_2^R(t)$. (b) On a different scale along the vertical axis (appearing on the right), the time evolution of the single-particle second-rank orientational time correlation function $C_2^s(t)$ is shown in a log-log plot for the two temperatures ($T=3.0$ and 2.75) that are closest to the I-N transition on either side along with the time evolution of $\alpha_2^R(t)$. Solid and dotted lines are used for the same purpose as in Fig. 1.

$=\boldsymbol{\phi}_i(t)-\boldsymbol{\phi}_i(0)=\int_0^t dt' \boldsymbol{\omega}(t')$, ω_i being the corresponding angular velocity [13,14], and N is the number of ellipsoids of revolution in the system. The NGP will have a value equal to zero when the system dynamics is spatially homogeneous and will have a nonzero value when the system dynamics is spatially heterogeneous. As a typical behavior, Figs. 3(a) and 3(b) show the time dependence of the rotational NGP for one of the systems at several temperatures across the I-N transition along an isochor. On approaching the I-N transition upon cooling, a bimodal feature starts appearing with the growth of a second peak, which eventually becomes the dominant one, at longer times.

We further investigate the appearance of this bimodal feature in the NGP plot. To this end we calculate the mean-square angular deviation (MSAD) of the system at different temperatures starting from the high-temperature isotropic phase to the low-temperature nematic phase. The appearance of the bimodal feature in the rotational NGP is accompanied by a signature of a subdiffusive regime in the temporal evolution of the MSAD, the time scale of the short-time peak and that of the onset of the subdiffusive regime being comparable, as shown in Fig. 3(a). We note that the dominant peak appears on a time scale which is comparable to that of the onset of diffusive motion in orientational degrees of freedom (ODOF) as evident in Fig. 3(a). A similar feature has been observed recently for supercooled water [20]. We further find that the time scale at which the long-time peak appears is also comparable to the time scale of the onset of the plateau that is observed in the time evolution of $C_2^s(t)$, as shown in Fig. 3(b).

A. Mode-coupling theory analysis

This striking similarities of the dynamics between liquid crystals near I-N transition and supercooled liquid near the glass transition are also supported by the use of mode-coupling theory (MCT) to explain the dynamics of both the systems. While MCT was used first for the supercooled liquid, recently it has been used for liquid crystals also. MCT developed by Gottke *et al.* [3] predicts that near the I-N transition, the low-frequency rotational memory kernel should diverge in a power-law fashion:

$$M_R(z) \approx \frac{A}{z^\alpha}. \tag{11}$$

A mean-field treatment gives $\alpha=0.5$. Invoking the rank (l) dependence of the memory function, the single-particle OTCF can be written as [21–24]

$$C_l^s(z) = \left[z + \frac{l(l+1)k_BT}{I[z+\Gamma_l(z)]} \right]^{-1}. \tag{12}$$

The above equation can be Laplace inverted to obtain a short-to-intermediate power-law decay in $C_2^s(t)$ which is a universal characteristic of the I-N transition for several model liquid crystals [5,6,12]. Recently, Li *et al.* [25] showed that it is also possible to formulate a schematic model that combines short-to-intermediate-time relaxation with long-time relaxation. In their model, they have expressed the total memory function $[M(t)]$ as the sum of the mode-coupling memory function $[M_{MCT}(t)]$ and Landau–de Gennes (LdG) memory function $[M_{LdG}(t)]$:

$$M(t) = M_{MCT}(t) + M_{LdG}(t), \tag{13}$$

where

$$M_{MCT}(t) = \Omega^2 K(t), \tag{14}$$

Ω is the characteristic frequency, and $K(0)=1$. The time dependence of $K(t)$ can be expressed in terms of the memory function $m(t)$ [25], and $m(t)$ has the form

$$m(t) = \kappa \phi(t) \phi_1(t), \tag{15}$$

where $\phi(t)$ is the autocorrelation function of the anisotropy of the polarizability and $\phi_1(t)$ is the solution of a F_{12} schematic model for what is referred to as the density correlator,

κ being the coupling constant between them. Now, $M_{LdG}(t)$ can be written as

$$M_{LdG}(t) = \Gamma \delta(t). \tag{16}$$

Here Γ^{-1} is the relaxation time ($\Gamma^{-1} = \tau_{LdG}$) and it diverges as $(T - T^{\star})^{-1}$ as the critical temperature $T^{\star}$ of the I-N transition is approached from above. Following the calculation of Ref. [25], one can get two important relaxation equations

$$\ddot{\phi}_1(t) = -\Omega_1^2 \phi_1(t) - \mu_1 \dot{\phi}_1(t) - \Omega_1^2 \int_0^t dt' m_1(t-t') \dot{\phi}_1(t'), \tag{17}$$

with the initial conditions $\phi_1(0) = 1$ and $\dot{\phi}_1(0) = 0$, and

$$\ddot{\phi}(t) = -(\Omega^2 + \mu\Gamma)\phi(t) - (\mu + \Gamma)\dot{\phi}(t) - \Omega^2 \times \int_0^t dt' m(t-t')\dot{\phi}(t') - \Omega^2 \Gamma \int_0^t dt' m(t-t')\phi(t'), \tag{18}$$

with the initial conditions $\phi(0) = 1$ and $\dot{\phi}(0) = -\Gamma$. Here μ_1 and μ are the damping constants. Equation (17) is identical to what one gets from a MCT analysis of supercooled liquids. The difference between this schematic model and the one applied to the supercooled liquid is in Eq. (18). If Γ is set equal to 0 in Eq. (18), the supercooled model is recovered. Equation (18) is the orientational correlation function coupled to the density correlation function with specific new terms that account for the long-time portion of the relaxation profile that has been previously described by LdG theory.

B. Energy landscape analysis

Several studies have attempted to interpret the fragility of glass-forming liquids in terms of the features of the underlying energy landscapes [26–31]. Energy landscape analysis gives the potential energy, which is devoid of any kind of thermal motion, of inherent structures of the parent liquid and hence provides a better understanding of the structure and dynamics of the parent liquid. A recent study of thermotropic liquid crystals has reported the temperature-dependent exploration of the energy landscapes of a family of the Gay-Berne model systems across the mesophases [10]. The average inherent structure (IS) energy $\langle e_{IS} \rangle$ has been found to fall as $\langle S \rangle$ grows across the I-N phase boundary and through the nematic phase in contrast to its insensitivity to the temperature in the high-temperature isotropic phase and the low-temperature smectic-B phase [10]. Such a fall in the average IS energy is consistent with a Gaussian form for the number density of inherent structures with energy e_{IS}, which predicts a linear variation of $\langle e_{IS} \rangle$ with the inverse temperature: $\langle e_{IS} \rangle(T) = e_{IS}^0 - \sigma^2 / 2Nk_BT$, where e_{IS}^0 and σ are parameters independent of temperature and k_B is the Boltzmann constant [29]. Note that this has been observed for a glassy system [29], where the average IS energy also falls over a temperature range [27]. It is, however, important to recognize that the non-Gaussian parameter which is used to diagnoze heterogeneous dynamics is a measure of the deviation from the Gaussian behavior in dynamical variables rather than the distribution of inherent structure energy. In Fig. 4(a), we demonstrate with the original and most studied parametrization for the GB pair potential GB(3,5,2,1) that the prediction holds good over the temperature range where $\langle e_{IS} \rangle$ is on a decline along all three isochors studied. It then follows that a plot of $\langle e_{IS} \rangle(T) - e_{IS}^0$ versus $\sigma^2 / 2Nk_BT$ would result in a collapse of the $\langle e_{IS} \rangle$ data for all densities onto a straight line with negative unit slope. This is indeed found to be true, as shown in Fig. 4(b), implying the validity of the Gaussian model in this case as well. It may be noted that when the distribution of IS energy is Gaussian, the fragility of glass-forming liquids has been shown to depend on the total number of inherent structures, the width of the Gaussian, and the variation of the basin shape with the average IS energy [29].

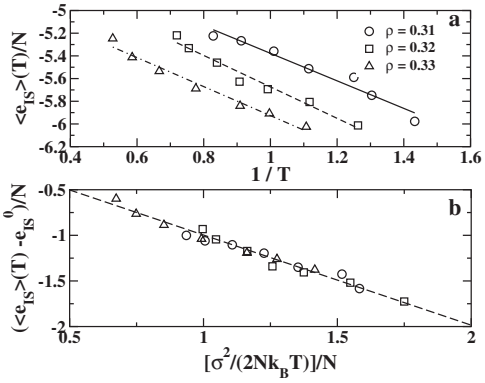

FIG. 4. The energy landscapes as explored by the system with the aspect ratio 3 on variation of temperature along three isochors. (a) The average inherent structure (IS) energy per particle as a function of the inverse temperature at different densities. The solid line, dashed line, and dot-dashed line are the linear fits to the data at the densities ρ=0.31, 0.32, and 0.33, respectively. (b) The displaced average IS energy per particle versus a scaled inverse temperature along the same three isochors. If the Gaussian model for the number density of the IS energy with a given energy is validated, a collapse of the data for all densities is expected onto a straight line with negative unit slope, which is drawn. The data are shown over the temperature regimes in which the average IS energy is on a decline.

IV. CONCLUSION

The origin of the glassy orientational dynamics, both single-particle and collective, of mesogens near the isotropic-nematic transition has been addressed in several publications in recent years [3–5,10]. In these studies, the similarity between dynamics of supercooled liquids and liquid crystals has been discussed in detail, but no quantitative measure of the same has been provided. The fragility index introduced here serves to remove that lacuna. It is indeed surprising that even the values of the fragility parameter are in the range observed for glassy liquids as well. This is in agreement with the observation by Cang *et al.* [4] that the values of the power-law exponents observed in the two systems are quite similar. Further understanding of the relax-

ation mechanism has been obtained from a closer look on the heterogeneous dynamics. As Fig. 3 demonstrates, the rotational non-Gaussian parameter shows a dramatic enhancement of heterogeneous dynamics as the I-N phase boundary is approached upon cooling. Unlike what is found near the gas-liquid critical point [32], the single-particle dynamics near the I-N phase boundary is observed to be strongly affected by the approaching thermodynamic singularity. We have also discussed mode-coupling theory approaches introduced to understand anomalous dynamics observed in this problem.

ACKNOWLEDGMENTS

It is a pleasure to thank Professor S. Sastry for helpful discussions. This work was supported in parts by grants from DST and CSIR, India. B.J. acknowledges CSIR, India, and D.C. acknowledges UGC, India, for support.

[1] P. G. de Gennes and J. Prost, *The Physics of Liquid Crystals* (Clarendon Press, Oxford, 1993).
[2] S. Chandrasekhar, *Liquid Crystals* (Cambridge University Press, Cambridge, England, 1992).
[3] S. D. Gottke, H. Cang, B. Bagchi, and M. D. Fayer, J. Chem. Phys. **116**, 6339 (2002).
[4] H. Cang, J. Li, V. N. Novikov, and M. D. Fayer, J. Chem. Phys. **118**, 9303 (2003).
[5] P. P. Jose, D. Chakrabarti, and B. Bagchi, Phys. Rev. E **71**, 030701(R) (2005).
[6] S. Chakrabarty, D. Chakrabarti, and B. Bagchi, Phys. Rev. E **73**, 061706 (2006).
[7] J. G. Gay and B. J. Berne, J. Chem. Phys. **74**, 3316 (1981).
[8] M. A. Bates and G. R. Luckhurst, J. Chem. Phys. **110**, 7087 (1999).
[9] J. M. Ilnytskyi and M. R. Wilson, Comput. Phys. Commun. **148**, 43 (2002).
[10] D. Chakrabarti and B. Bagchi, Proc. Natl. Acad. Sci. U.S.A. **103**, 7217 (2006).
[11] C. Zannoni, in *Advances in the Computer Simulations of Liquid Crystals*, edited by P. Pasini and C. Zannoni (Kluwer Academic, Dordrecht, 2000).
[12] D. Chakrabarti, P. P. Jose, S. Chakrabarty, and B. Bagchi, Phys. Rev. Lett. **95**, 197801 (2005).
[13] S. Kämmerer, W. Kob, and R. Schilling, Phys. Rev. E **56**, 5450 (1997).
[14] C. De Michele and D. Leporini, Phys. Rev. E **63**, 036702 (2001).
[15] C. A. Angell, J. Phys. Chem. Solids **49**, 863 (1988).
[16] C. A. Angell, J. Non-Cryst. Solids **131-133**, 13 (1991).
[17] R. Böhmer, K. L. Ngai, C. A. Angell, and D. J. Plazek, J. Chem. Phys. **99**, 4201 (1993).
[18] M. D. Ediger, Annu. Rev. Phys. Chem. **51**, 99 (2000).
[19] M. S. Shell, P. G. Debenedetti, and F. H. Stillinger, J. Phys.: Condens. Matter **17**, S4035 (2005).
[20] M. G. Mazza, N. Giovambattista, F. W. Starr, and H. E. Stanley, Phys. Rev. Lett. **96**, 057803 (2006).
[21] S. Ravichandran and B. Bagchi, Int. Rev. Phys. Chem. **14**, 271 (1995).
[22] B. Bagchi and A. Chandra, Adv. Chem. Phys. **80**, 1 (1991).
[23] J. B. Hubbard and P. G. Wolynes, J. Chem. Phys. **69**, 998 (1978).
[24] B. Bagchi, J. Mol. Liq. **77**, 177 (1998).
[25] J. Li, H. Cang, H. C. Andersen, and M. D. Fayer, J. Chem. Phys. **124**, 014902 (2006).
[26] D. J. Wales, *Energy Landscapes* (Cambridge University Press, Cambridge, England, 2003).
[27] S. Sastry, P. G. Debenedetti, and F. H. Stillinger, Nature (London) **393**, 554 (1998).
[28] A. Scala, F. W. Starr, E. L. Nave, F. Sciortino, and H. E. Stanley, Nature (London) **406**, 166 (2000).
[29] S. Sastry, Nature (London) **409**, 164 (2001).
[30] L.-M. Martinez and C. A. Angell, Nature (London) **410**, 633 (2001).
[31] I. Salka-Voivod, P. H. Poole, and F. Sciortino, Nature (London) **412**, 514 (2001).
[32] R. Kutner, K. Binder, and K. W. Kehr, Phys. Rev. B **26**, 2967 (1982).